

# Multi-angular thermal infrared emission characteristics of Bohai Sea ice based on in situ measurements

Jinlong CHAO,<sup>1</sup> Chengyu LIU,<sup>2</sup> Yingjun XU,<sup>1</sup> Wei GU,<sup>1</sup> Ying LI,<sup>1</sup> Feng XIE<sup>2</sup>

<sup>1</sup>State Key Laboratory of Earth Surface Processes and Resource Ecology, Beijing Normal University, Beijing, China

<sup>2</sup>Key Laboratory of Space Active Opto-Electronics Technology, Shanghai Institute of Technical Physics, Chinese Academy of Sciences, Shanghai, China

Correspondence: Wei Gu <weigu@bnu.edu.cn>

**ABSTRACT.** We report on the radiative transfer process and optical properties of sea ice in the thermal infrared (TIR) band, presenting two new linear kernel driver models (Relative Emissivity Distribution Function, REDF) that describe TIR emission characteristics of smooth and rough ice. In order to test the models and determine the necessary coefficients, in situ measurements from the Bohai Sea were carried out during the 2011/12 and 2012/13 boreal winters. The results show that the relative emissivity of smooth sea ice decreases along with increasing viewing zenith angle, and the shape of the relative emissivity curve is similar to that of an ideal plane. Affected by parameters such as roughness and surface temperature distribution, the anisotropy of relative emissivity of sea ice with a high degree of roughness is stronger relative to the cosine emitter. The model coefficients were also obtained using a robust regression method based on the measured data. The presented models are more practical than the numerical radiative transfer model and can be used for multi-angular TIR remote sensing.

**KEYWORDS:** remote sensing, sea ice

## INTRODUCTION

The Bohai Sea, a continental sea of China (37°07′–41°00′ N, 117°35′–121°10′ E), is the southernmost sea in the Northern Hemisphere in which sea ice occurs during winter (Ding, 1999). Bohai Sea ice is first-year ice with an average thickness of 0.15–0.30 m and maximum thickness of 0.80–0.90 m. Affected by ocean currents, tide and wind, Bohai Sea ice is in continuous motion. Collision, overlapping and extrusion occur during sea-ice movement, resulting in a concave–convex or deformed surface. The majority of Bohai Sea ice is rough; the sea ice in harbours and bays is relatively smooth (Ding, 1999). For clarity, we define smooth ice as ice where surface variations are <0.01 m, and rough ice as applying to all other ice types and conditions.

The Bohai coastal area is an important economic zone of northern China, with many cities, a dense population and heavy traffic. The emergence of sea ice has a negative impact on marine traffic, aquaculture and the ecological environment. Winter sea ice has caused major ocean disasters in the Bohai Sea (Omstedt, 1990; Launiainen and Cheng, 1998; Gu and others, 2013; Liu and others, 2013).

Fast, accurate information on sea-ice area and thickness is essential to prevent or limit sea-ice disasters and to optimize use of resources. The Bohai Sea (area 77 000 km<sup>2</sup>) has been monitored on a large scale in real time using remote-sensing products comprising different satellite data or airborne data (Ding, 1999). Ice thickness is one of the major components of remote-sensing monitoring. Based on Yang (2000), Luo and others (2004), Wu and others (2006) and Yuan and others (2012), the thickness of smooth sea ice can be inverted using the correlation of reflectance between ice thickness and visible/near-infrared (VNIR) reflectance. Rough ice surfaces increase the anisotropic scattering from incoming solar radiation, which distorts the correlation of reflectance between ice thickness and the VNIR spectrum. Consequently, the inversion error of ice thickness increases

to 20–30% in the Bohai Sea (Li and others, 2012). One possible approach to solving this problem is to explore whether bands other than VNIR, such as the thermal infrared (TIR) band, are able to invert the surface roughness. In the TIR band, pixel TIR emissions received by the sensor from any particular direction are closely related to the local viewing zenith angle and azimuth angle of each point of the ice surface. Therefore, multi-angular TIR remote sensing can detect the surface roughness. Such an approach can then be used to correct the sea-ice thickness error through a model based on VNIR remote-sensing data.

The primary step to realize this is to verify the response of TIR emissions from sea ice against roughness measurements obtained through field observations. However, most TIR remote-sensing studies of sea ice concentrate on the measurement of TIR radiation characteristics of sea ice in polar regions, and on the inversion of sea-ice thickness with a thermodynamic model (Groves and Stringer, 1991; Comiso, 2001; Masahiro and others, 2006; Kaleschke and others, 2012). Our study concentrates mainly on research using single-angle TIR imagery to calculate sea-ice thickness and area (Zheng and others, 1998; Yang, 2000). To our knowledge, there is no previously reported field study of multi-angular TIR remote sensing of Bohai Sea ice; there has been some research in eastern Hokkaido, Japan (Masahiro and others, 2006).

We report observations of radiation brightness temperature of sea ice for rough and smooth types and from different observation directions, which we convert to radiance. Ignoring path radiance, absorption and atmospheric scattering between sensor and sea-ice surface, we calculate the relative emissivity from different directions. Based on the radiation transfer equation, the relative emissivity of the ice under each viewing zenith angle is calculated, and the characteristics of the change in relative emissivity, along with changes in sea-ice roughness and viewing zenith angle, are analysed. Finally, using a robust regression method, we

create a linear kernel driver model called a Relative Emission Distribution Function (REDF) to describe different roughnesses.

**PRINCIPLES**

**Radiation received by sensor**

Bohai Sea ice consists of a mix of ice types which contain brine bubbles and bubbles and other impurities. Except for bubbles and impurities with relatively low emissivity, the emissivity of brine bubbles and pure ice is relatively high, and pure ice accounts for the highest proportion of volume. Usually the average emissivity of sea ice is ~0.97 (Drüe and Heinemann, 2005), with Kirchhoff’s law showing that the absorptivity (absorption capacity) of sea ice is very high. Internal TIR emission from sea ice is basically absorbed by itself. The TIR emission of the sea-ice surface mainly comes from a very thin micron-sized surface layer, i.e. the ‘skin’ effect (Xu, 2006; Kuenzer and Dech, 2013).

The high absorptivity of sea ice leads to extremely shallow (<1 mm) penetration of TIR emissions. Compared with the VNIR spectrum, this absorptivity eliminates complicated radiative transfer processes within the ice, although temperatures on the ice surface may be heterogeneous. The sea-ice surface radiation energy received by the sensor is described using the Li–Strahler–Friedl (LSF) conceptual model (Li and others, 1999, 2001):

$$L(\theta_v, \phi_v) = \frac{\iint_A \varepsilon_s(\theta_L, \phi_L) B(T_s) \langle \vec{s}, \vec{r} \rangle I(\vec{s}, \vec{r}) ds}{A \cos(\theta_v)} + \frac{\iint_A \widehat{\Delta L}_s [1 - \varepsilon_s(\theta_L, \phi_L)] \langle \vec{s}, \vec{r} \rangle I(\vec{s}, \vec{r}) ds}{A \cos(\theta_v)} + \frac{\iint_A \iint_{2\pi} L_a^{\downarrow}(\theta, \phi) I(\theta, \phi, \vec{s}) d\theta d\phi [1 - \varepsilon_s(\theta_L, \phi_L)] \langle \vec{s}, \vec{r} \rangle I(\vec{s}, \vec{r}) ds}{A \cos(\theta_v)} \tag{1}$$

where  $L(\theta_v, \phi_v)$  is the radiance received in the observation direction of  $(\theta_v, \phi_v)$ ,  $A$  is pixel area,  $B(T_s)$  is the radiance of the isothermal black body for isothermal patch  $ds$ ,  $T_s$  is surface temperature,  $\varepsilon_s(\theta_L, \phi_L)$  is the emissivity of patch  $ds$  in the direction of  $(\theta_L, \phi_L)$ ,  $\theta_L$  and  $\phi_L$  are the viewing zenith angle and azimuth angle of observation direction of the sensor relative to patch  $ds$  respectively,  $\langle \vec{s}, \vec{r} \rangle$  is the cosine value of the intersection angle between the normal vector and viewing direction vector,  $\vec{s}$  is the normal vector of patch  $ds$ ,  $\vec{r}$  is the observation direction vector,  $I(\vec{s}, \vec{r})$  is the visibility from patch  $ds$  to the sensor,  $I(\theta, \phi, \vec{s})$  is the visibility of atmospheric downward radiation relative to the patch  $ds$  (for sea ice,  $\{0, 1\}$  can be taken),  $L_a^{\downarrow}(\theta, \phi)$  is the downward TIR radiation of the atmosphere and  $\widehat{\Delta L}_s$  is the increment caused by reflection between patches. Considering only the one-time contribution of other surface patches to  $ds$ ,  $\widehat{\Delta L}_s$  can be abbreviated as

$$\widehat{\Delta L}_s \approx \iint_A B(T_{s_1}) \varepsilon_{s_1}(\theta_{s \rightarrow s_1}) I(s, s_1) ds_1 \tag{2}$$

where  $B(T_{s_1})$  is the radiance of the isothermal black body for isothermal patch  $ds_1$ ,  $T_{s_1}$  is surface temperature,  $\varepsilon_{s_1}(\theta_{s \rightarrow s_1})$  is the emissivity of patch  $ds_1$  in the direction of angle  $\theta_{s \rightarrow s_1}$ ,  $\theta_{s \rightarrow s_1}$  is the intersection angle between the line of centres of  $ds - ds_1$  and the normal vector of panel  $ds_1$ ,  $B(T_{s_1}) \varepsilon_{s_1}(\theta_{s \rightarrow s_1})$  can be considered as the radiation energy from patch  $ds_1$  to

**Table 1.** Units of variables

Variable	Description	Unit
$L$	Radiance	$W m^{-2} \mu m^{-1} sr^{-1}$
$\theta$	Viewing zenith	$^{\circ}$
$\varphi$	Azimuth	$^{\circ}$
$\varepsilon$	Emissivity	dimensionless
$I$	Relative visibility	dimensionless
$B$	Radiance	$W m^{-2} \mu m^{-1} sr^{-1}$
$T_s$	Surface temperature	$^{\circ}C$
$\vec{s}$	Normal vector of patch	$\vec{e}$
$T_{SIS}$	Surface temperature	$^{\circ}C$
$\vec{r}$	Observation direction vector	$\vec{e}$
$\rho$	Density function	dimensionless
$s$	Gradient	dimensionless
$J$	Coefficient of REDF	dimensionless
DHR	Directional-hemispherical reflectance	dimensionless
$\gamma$	Fresnel reflectance	dimensionless
$\rho_{\Omega}$	Directional-hemispherical reflectance	dimensionless
$\sigma$	Root-mean-squared height (RMSH)	m
$k$	Kernel function	dimensionless
$F$	Integral of kernel function	dimensionless
$J_1$	Coefficient of REDF	dimensionless
$J_2$	Coefficient of REDF	dimensionless

$ds$  and  $I(s, s_1)$  is the visibility. The units of variables used are listed in Table 1.

As can be seen from Eqns (1) and (2), radiation energy received by the sensor is related to the actual temperature of the patch, the projected area of the patch within the field of view of the sensor, and the multiple reflections between patches. Equation (1) illustrates the composition and generation mechanism of sea-ice TIR radiation transmission received by the sensor. However, to accurately calculate  $L(\theta_v, \phi_v)$ , it is necessary to know the temperature of the patch  $ds$ , multiple angle radiation characteristics of the patch (directional relative emissivity), and sea-ice surface conditions. Equations (1) and (2) indicate that the sea-ice radiation characteristics are affected by surface conditions and distribution of surface temperature, both of which involve relatively complicated processes.

The accuracies of the parameters for sea-ice surface temperature and roughness retrieved using single-angle remote-sensing data cannot meet the application demand. However, TIR remote sensing can collect the radiance from multiple observation directions and provide more sampling data, with more complete sampling than single-angle measurements. This additional resource can further improve the accuracies of sea-ice roughness and temperature estimates from TIR remote sensing.

**Relative emissivity**

Given the short distance between sensor and sea-ice surface (~2 m), the path radiance, absorption and atmospheric scattering between sensor and sea-ice surface can be ignored (Xu, 2006). If the sea-ice surface is isothermal, the sea-ice TIR radiation transfer equation can be simplified to

$$L(\theta_v, \phi_v) = \varepsilon(\theta_v, \phi_v) B(T_{SIS}) + [1 - \varepsilon(\theta_v, \phi_v)] L_a^{\downarrow} \tag{3}$$

where  $\varepsilon(\theta_v, \phi_v)$  is the emissivity of sea ice in the  $(\theta_v, \phi_v)$  direction,  $B(T_{SIS})$  is the radiation of the black body corresponding to the sea ice and  $T_{SIS}$  is the sea-ice surface temperature, i.e. average temperature of pixels (Li and others, 2013).

**Table 2.** Characteristics of the smooth sea-ice samples

Sample	Thickness m	Appearance
Smooth 1	0.15	Smooth surface, opaque white
Smooth 2	0.34	Relatively smooth, transparent surface
Smooth 3	0.09	Tiny ups and downs on surface, transparent and darker, with frazil ice
Smooth 4	0.40	Millimetre-sized ups and downs on surface, opaque white
Smooth 5	0.37	Relatively smooth, rendered opaque white
Smooth 6	0.35	Smooth surface, transparent white, with frazil ice

It is difficult to measure the temperature of each point of the sea-ice surface. For water bodies, we can only measure the surface temperature of the homogeneous and isothermal mass (Li and others, 2013). In Eqn (3), the first term on the right-hand side is the radiation energy of sea ice with surface temperature  $T_{\text{SIS}}$ , and the second term is the downward radiation energy of the whole atmospheric layer, which is reflected to the field of view of the instrument. The term  $[1 - \varepsilon(\theta_v, \phi_v)]$  is equivalent to the directional-hemispherical reflectance. Here we assume that hemispherical-directional reflectance (the ratio of the energy reflected in the specific direction to the energy incident on the surface from all directions) is equal to directional-hemispherical reflectance.

By converting Eqn (3), the emissivity equation can be expressed as

$$\varepsilon(\theta_v, \phi_v) = \frac{L(\theta_v, \phi_v) - L_a^\downarrow}{B(T_{\text{SIS}}) - L_a^\downarrow} \quad (4)$$

It can be seen from Eqn (4) that, in order to accurately calculate the emissivity when the observation direction is  $(\theta_v, \phi_v)$ , it is necessary to obtain the values of the three parameters  $L(\theta_v, \phi_v)$ ,  $L_a^\downarrow$  and  $B(T_{\text{SIS}})$  to a known accuracy. As stated above, it is still difficult to accurately measure sea-ice surface temperature, and it is also difficult to calculate  $B(T_{\text{SIS}})$ . If  $L_0$  and  $\varepsilon_0$  are, respectively, the radiance and emissivity at the viewing angle,  $0^\circ$ , using  $L_0/\varepsilon_0$  to express  $B(T_{\text{SIS}})$ , Eqn (4) can be simplified to

$$\varepsilon(\theta_v, \phi_v) = \frac{L(\theta_v, \phi_v) - L_a^\downarrow}{B(T_{\text{SIS}}) - L_a^\downarrow} = \frac{\varepsilon_0 [L(\theta_v, \phi_v) - L_a^\downarrow]}{L_0 - \varepsilon_0 L_a^\downarrow} \quad (5)$$

If

$$\varepsilon(\theta_v, \phi_v) = \varepsilon_r(\theta_v, \phi_v) \cdot \varepsilon_0 \quad (6)$$

then Eqn (5) can be expressed as

$$\varepsilon_r(\theta_v, \phi_v) = \frac{L(\theta_v, \phi_v) - L_a^\downarrow}{L_0 - \varepsilon_0 L_a^\downarrow} \quad (7)$$

We call  $\varepsilon_r(\theta_v, \phi_v)$  the relative emissivity in the direction  $(\theta_v, \phi_v)$  (Garcia and others, 2009), i.e. the emissivity relative to the viewing zenith angle,  $0^\circ$ . With  $\varepsilon_0 \rightarrow 1$  and with a very small magnitude of  $L_a^\downarrow$ , the following approximate equation can be used with the right-hand side of Eqn (7):

$$\frac{L(\theta_v, \phi_v) - L_a^\downarrow}{L_0 - \varepsilon_0 L_a^\downarrow} \approx \frac{L(\theta_v, \phi_v) - L_a^\downarrow}{L_0 - L_a^\downarrow}$$

Therefore, the relative emissivity can be simplified further to

$$\varepsilon_r(\theta_v, \phi_v) = \frac{L(\theta_v, \phi_v) - L_a^\downarrow}{L_0 - L_a^\downarrow} \quad (8)$$

Thus, we can calculate the relative emissivity of sea ice by only measuring  $L(\theta_v, \phi_v)$  and  $(L_a^\downarrow(\theta \in [0, 90], \phi \in [0, 360]))$ . Relative emissivity is a non-dimensional parameter, which has a closer relation to the distribution characteristics of sea-ice radiation energy in  $2\pi$  space, i.e. it is more easily affected by sea-ice roughness and temperature distribution characteristics.

## EXPERIMENTS

### Instrument

The instrument used for the experiment is a TH3102 MR TIR imager produced by SAN-EI Company Limited of Japan. The working wavelength range of the instrument is 8–13  $\mu\text{m}$ , with a temperature resolution of 0.02°C, spatial resolution of 1.5 mrad, Stirling refrigeration, and nominal measurement accuracy of  $\pm 5\%$ . The TIR imager used was calibrated with a black-body source with high precision in the laboratory, and the system error correction was also made beforehand. We thus believe that the TIR imager system deviation was very small during the measurement and can be neglected. To eliminate random error as far as possible, data were averaged over ten observations for the result value in each measurement. The instrument consists of two parts, detectors and controllers, with a horizontal field-of-view (FOV) angle of  $30^\circ$  and vertical FOV angle of  $28.5^\circ$ . The pseudo-colour result display was adopted by the controller along with radiance brightness temperature output. A sensor is fixed on the observing scaffold at height 2 m. We used a high-accuracy IMPULSE 200 laser rangefinder. The ranging accuracy was 0.03 m and angular accuracy was  $0.1^\circ$ . The distance for rough ice is measured from the sensor's centre to the centre of the ice sample. When the viewing zenith angle is  $0^\circ$ , its field coverage is 1 m  $\times$  1 m. The dimension of each pixel is  $\sim 2$  mm.

### Experimental scheme

A field experiment was conducted near the Jiangjunshi fishing port, Xiyang Township, Wafangdian City, Liaoning province ( $39^\circ 55' 14''$  N,  $121^\circ 40' 48''$  E; Fig. 1). According to past sea-ice survey results in the Bohai Sea (Ding, 1999), both ice thickness and roughness are larger near the coast; the field site is reasonably representative. We conducted the experiments on smooth ice from 14 January to 8–9 February 2012 and on rough ice from 24 to 26 January 2013. The measurement period was during the sea-ice maximum in the Bohai Sea.

#### Smooth sea-ice experiment scheme

Smooth sea ice always forms in static sea water, while rough ice forms in moving sea water. The surveys showed that the root-mean-squared height (RMSH) of smooth sea-ice samples was  $< 0.01$  m, but rough ice in the Bohai Sea always formed from the crushed smooth sea ice, while for rough ice the RMSH is  $> 0.01$  m. Six samples of typical smooth sea ice (Smooth 1–Smooth 6) were selected for measurement (Table 2; Fig. 2). Since the change of relative emissivity along with the change of azimuth angle is very small ( $< 0.01$ ) (Fig. 3), only  $90^\circ$  viewing azimuth is recorded. There are nine viewing zenith angles, in  $10^\circ$  intervals from  $0^\circ$  to  $80^\circ$ .

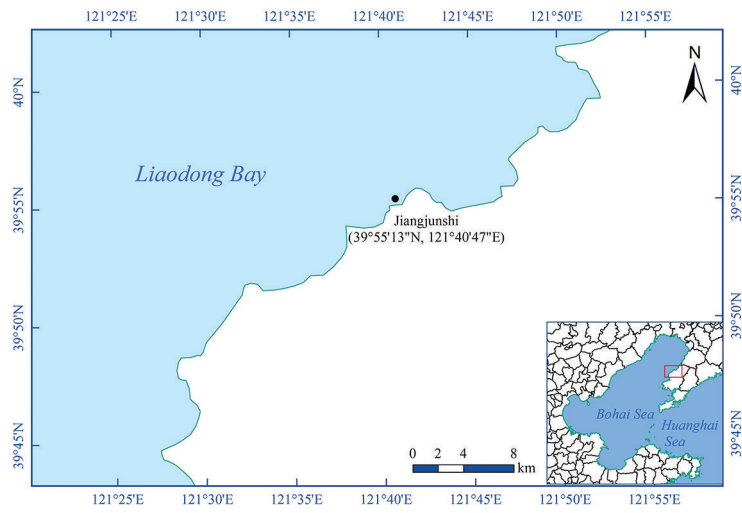


Fig. 1. The measurement site.

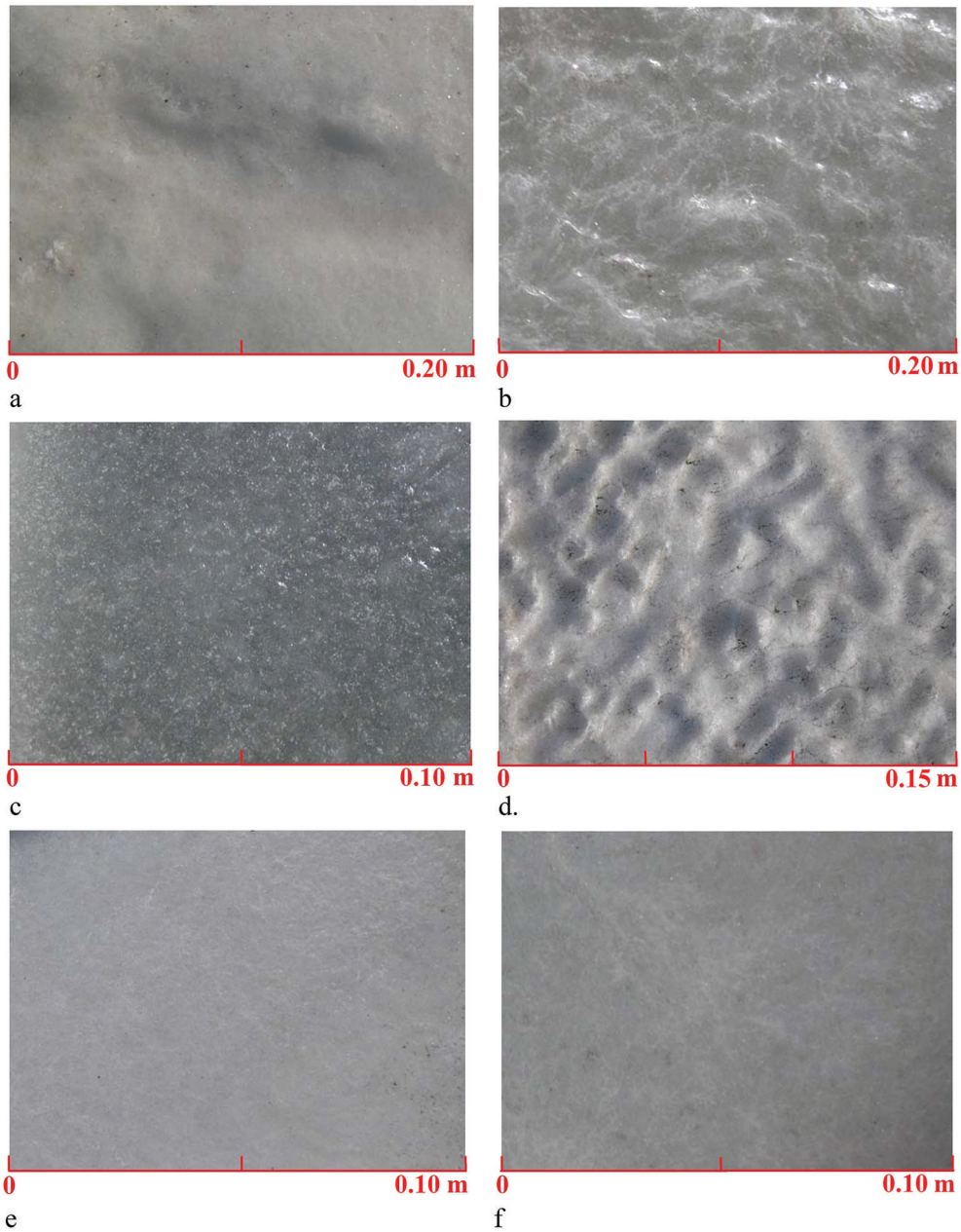
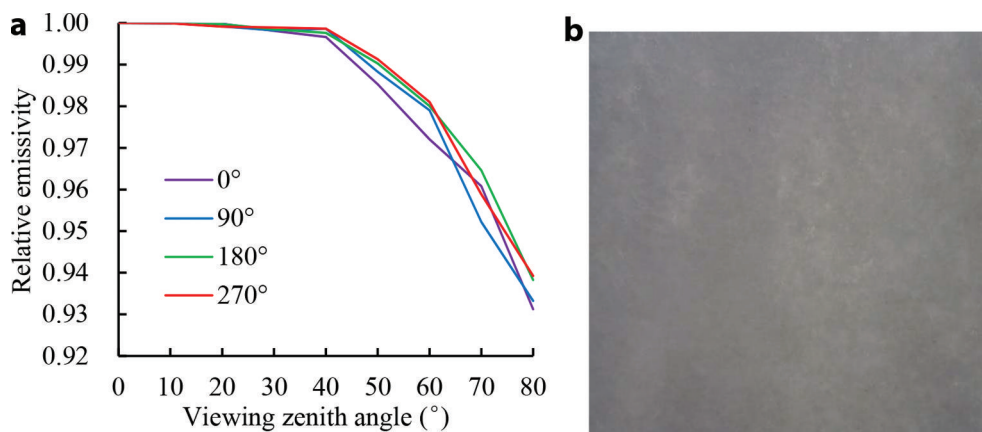


Fig. 2. (a–f) Photographs of smooth sea-ice samples 1–6.



**Fig. 3.** Measured smooth sea-ice relative emissivity (sea-ice thickness is 0.20 m). (a) Plot of relative emissivity with 0°, 90°, 180° and 270° mean viewing azimuths. (b) Photograph of sea-ice sample.

A UIRT-94-050 TIR diffuse plate produced by the Labsphere Company is used to measure  $L_a^\perp$  in Eqn (8). The hemispherical reflectance of the UIRT-94-050 TIR diffuse plate in the TIR direction is 0.94. Thus, the actual  $L_a^\perp$  is calculated by

$$L_a^\perp = \frac{L_{\text{panel}} - \varepsilon_{\text{panel}} B(T_{\text{panel}})}{1 - \varepsilon_{\text{panel}}} \quad (9)$$

where  $L_{\text{panel}}$  is the radiance of the diffuse reflection plate received by the instrument,  $\varepsilon_{\text{panel}}$  is the relative emissivity of the diffuse plate and  $B(T_{\text{panel}})$  is the corresponding radiance of the black body of the diffuse plate.

In actual measurement, the major steps are:

1. measurement of radiation brightness temperature of the diffuse plate, with a viewing zenith angle of 40°, and measurement of temperature of the diffuse plate;
2. progressive measurement from 0° to 80°, with 10° viewing zenith angle intervals. Reflectance of the instrument during the measurement is set to be 1.0;
3. measurement of radiation brightness temperature and repeat measurement of the temperature of the diffuse plate.

A schematic diagram of the observation set-up is presented in Figure 4.

#### Rough sea-ice experiment

All the selected rough sea ice forms by collision, accumulation and congelation of smooth sea ice under the effects of current, wind, tide, etc. The experiment measured three sea-ice samples (Rough 1–Rough 3) of different roughness.

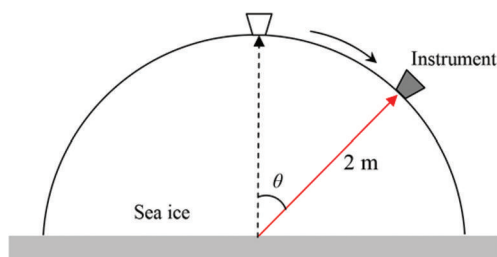


**Fig. 4.** Schematic diagram of TIR radiation observation of sea ice.

Using the laser scanner Trimble GX, we measured the point cloud from four measurement directions in the form of the root mean square (rms;  $\sigma$ ) of sea-ice surface variability (Table 3; Fig. 5). The viewing azimuths are 0°, 90°, 180° and 270°, and the viewing zenith angles are from 0° to 80° in 10° intervals, with a total of 33 observation directions. In Table 3,  $\sigma$  is the rms height of 100 selected profiles from the point cloud data of each sample, and is indicative of the roughness of the samples. The point cloud (the set of points with  $X$ ,  $Y$ ,  $Z$  coordinate values for describing the external surface of a ground-based feature) was measured with a Trimble GX 3D laser scanner. The main wavelength of the laser pulse is 532 nm, with a scan resolution of 3 mm at a distance of 50 m, and a 6.5 mm standard deviation at a distance of 200 m. There were hundreds of thousands of points in each sample.

Measurement steps are:

1. measurement of radiation brightness temperature of the diffuse plate, with a viewing zenith angle of 40°, and measurement of temperature of the diffuse plate;
2. progressive measurement with a viewing azimuth from 0° to 270° with intervals of 90°, and with viewing zenith angle from 0° to 80° with intervals of 10°. The reflectance of the instrument during measurements is set to be 1.0;
3. remeasurement of radiation brightness temperature and repeat measurement of the temperature of the diffuse plate.

A schematic diagram of the observation set-up is presented in Figure 6.

**Table 3.** Characteristics of rough sea-ice samples

Sample	Thickness* m	Roughness ( $\sigma$ ) m	Appearance
Rough 1	0.21	0.08	Consists of grey ice and white ice
Rough 2	0.25	0.12	White surface, with ice ridge
Rough 3	0.33	0.20	White surface, stranded ice on the shore

\*Thickness of lowest point of sea-ice surface.

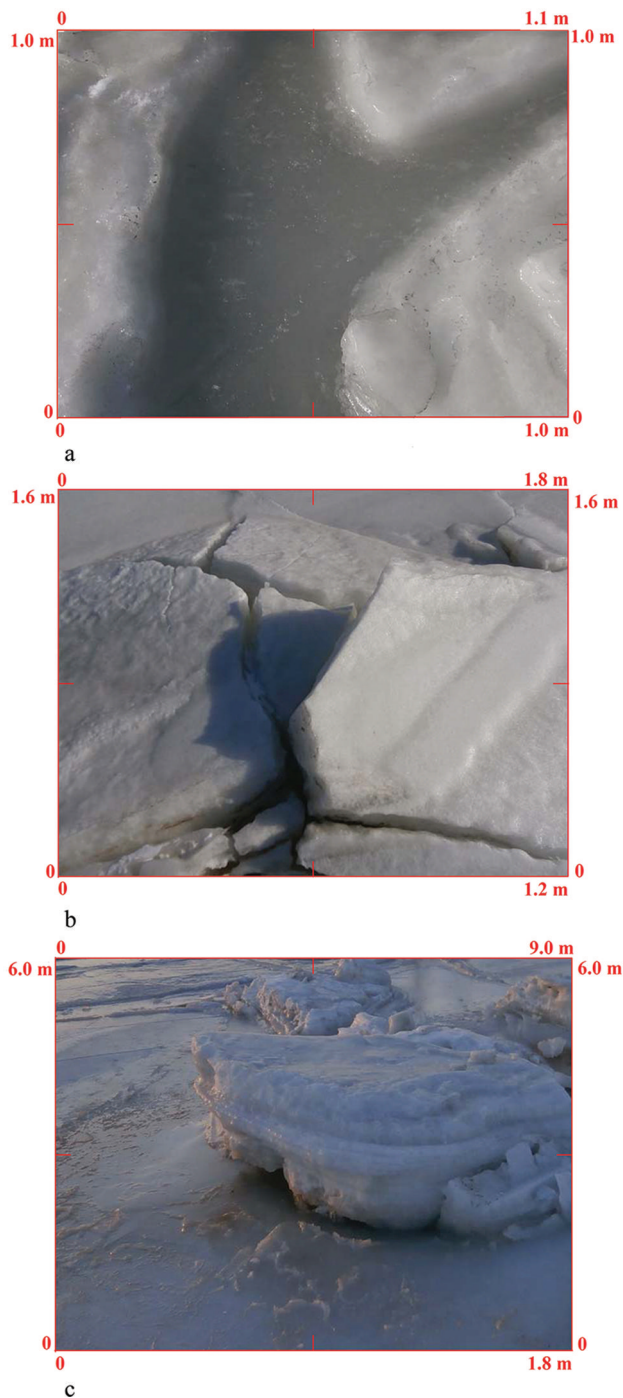


Fig. 5. (a–c) Photographs of rough sea-ice samples 1–3.

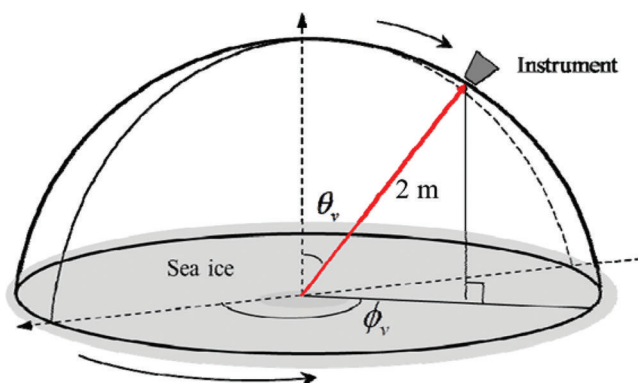
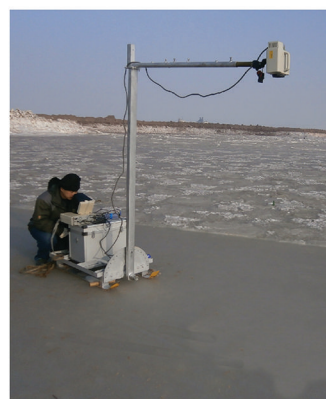


Fig. 6. Schematic diagram of TIR radiation observation of rough sea ice.



## RESULTS AND ANALYSIS

### Analysis of in situ measurements

#### Measured results of smooth sea ice

Figure 7 illustrates the relative emissivity under different viewing angles in the zenith direction. It shows that the relative emissivity of Smooth 3 at  $30^\circ$  is slightly larger than that at  $20^\circ$ , but the exact value is less than  $1/10000$  (0.00005) and may be due to measurement error. Relative emissivity at the other zenith angles is less than that at  $0^\circ$ . Relative emissivities of Smooth 4 at  $10^\circ$ ,  $20^\circ$ ,  $30^\circ$ ,  $40^\circ$  and  $50^\circ$  are  $>1.0$ , i.e. larger than the relative emissivity with a viewing zenith angle of  $0^\circ$ . However, when the viewing zenith angle is increased to  $80^\circ$ , relative emissivity quickly decreases to 0.963. Except for Smooth 3 and Smooth 4, the relative emissivity of other samples decreases along with the increase in viewing zenith angle. When the zenith angle is  $<50^\circ$ , the relative emissivity changes with viewing angle, showing a fluctuated pattern without a notable trend. When the viewing zenith angle is  $>50^\circ$ , relative emissivity decreases rapidly, with a minimum change rate for Smooth 2 ( $-0.001 \text{ degree}^{-1}$ ) and a maximum change for Smooth 6 ( $-0.003 \text{ degree}^{-1}$ ). Figure 7 shows that, except for the observation angle of  $50^\circ$ , the ranges of six samples at other observation angles increase with the increase in angle, while the maximum range is not that large (0.035).

#### Measured results for rough sea ice

Figure 8 shows the relative emissivity and ranges (viewing zenith angle) in different observation directions. Although the roughness values of the three samples differed, the relative emissivities decreased as the zenith angle increased when zenith angles were  $>60^\circ$ , and the order of the reduction was Rough 1  $>$  Rough 2  $>$  Rough 3, with less decrease with increasing roughness. The maximum and minimum relative emissivities of Rough 1 are respectively 1 and 0.915, with a difference of 0.085 (Fig. 8a); the maximum and minimum of Rough 2 are respectively 1.010 and 0.933, with a difference of 0.077 (Fig. 8b); the maximum and minimum of Rough 3 are respectively 1.081 and 0.973, with a difference of 0.108 (Fig. 8c). It is shown that the maximum and minimum relative emissivity increases as the roughness increases. This indicates that radiation energy at a large zenith angle increases with increase in roughness, which may sometimes be larger than that at a small zenith angle. Figure 8d shows the ranges of relative emissivity of three samples at different viewing zenith angles. The range of Rough 3 is largest, that of

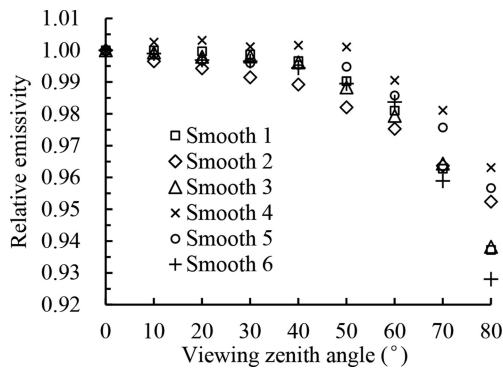


Fig. 7. Relative emissivity from different viewing zenith angles.

Rough 2 is smaller and that of Rough 1 is smallest. Rough 3, whose anisotropy of surface reflection characteristics and temperature distribution is strongest, has the largest roughness. Thus, Rough 3 has the largest anisotropy of TIR emission. The viewing azimuth of Rough 3 is 180°. There is a large step from the 50° to the 60° viewing zenith angle, and Rough 3 is a relatively extreme case. Due to the equipment and experiment conditions, we chose only three rough samples. Many more TIR emission measurement experiments concerning rough sea ice are required. The scatter diagrams of relative emissivity (Fig. 8) show that there are different combinations of radiation energy at different viewing azimuths, as the projected areas of the sections of sea ice on the sensor receiving plane are different. Eventually, this leads to large differences in relative emissivity, along with changing curves of viewing zenith angle at different viewing azimuths. The difference becomes

larger as roughness increases (Rough 3 > Rough 2 > Rough 1), i.e. the anisotropy in the horizontal direction increases.

**Relative emissivity distribution function (REDF) of sea ice**

It is assumed, based on Eqn (1) and lack of knowledge of multiple scatterings on the surface, that the patch *ds* is smooth and the radiation in the horizontal direction is uniform. If the gradient distribution on the known surface of the sea ice is  $p(s_x, s_y)$  and the temperature distribution at time *t* is  $p_t(T)$ , then Eqn (1) can be rewritten as

$$L(\theta_v, \phi_v) = \frac{\iint_A \iint \varepsilon_0 \varepsilon_r(\theta_L) B(T) p_t(T) p(s_x, s_y) \langle \vec{s}, \vec{r} \rangle I(\vec{s}, \vec{r}) \sqrt{1+s_x^2+s_y^2} ds_x ds_y dx dy}{A \cos \theta_v} \tag{10}$$

Here  $\varepsilon_s(\theta_L) = \varepsilon_r(\theta_L) \cdot \varepsilon_0$  is estimated from Eqn (6),  $\varepsilon_r(\theta_L)$  is the relative emissivity of the smooth sea ice and  $\varepsilon_r(\theta_L)$  is related to the height and slope under normal circumstances. If only the relationship with slope is considered, its probability density can be expressed as  $p_t(T|s_x, s_y)$ , and the specific form of  $p_t(T|s_x, s_y)$  can be obtained through field measurements.  $\langle \vec{s}, \vec{r} \rangle$  can be expressed as

$$\langle \vec{s}, \vec{r} \rangle = -\frac{s_x \sin \theta_v \cos \phi_v}{\sqrt{1+s_x^2+s_y^2}} - \frac{s_y \sin \theta_v \sin \phi_v}{\sqrt{1+s_x^2+s_y^2}} + \cos \theta_v$$

$\theta_L$  can be expressed as

$$\theta_L = \arccos \left( -\frac{s_x \sin \theta_v \cos \phi_v}{\sqrt{1+s_x^2+s_y^2}} - \frac{s_y \sin \theta_v \sin \phi_v}{\sqrt{1+s_x^2+s_y^2}} + \cos \theta_v \right)$$

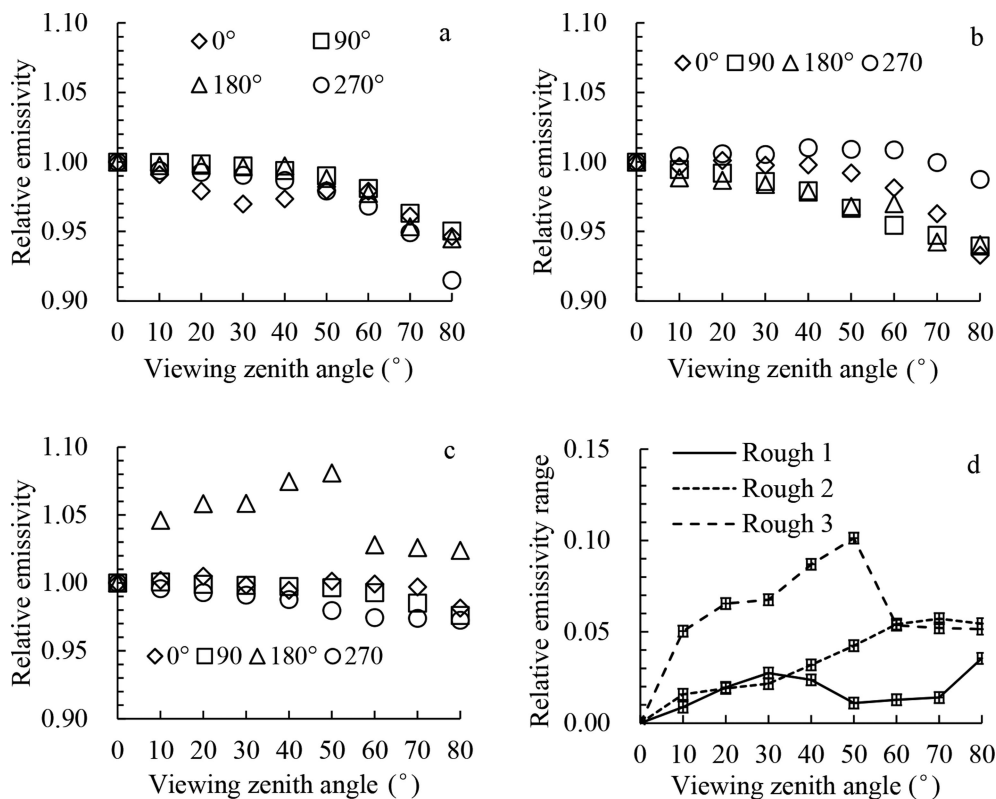


Fig. 8. Relative emissivity and ranges (zenith angle) in different samples in different viewing directions. (a–c) Samples Rough 1–Rough 3. (d) The range for each sample with error bar. The measuring error is 0.003, which was estimated from the uncertainties of the sensor and angle measurement.

and  $I(\vec{s}, \vec{r})$  can be expressed as

$$I(\vec{s}, \vec{r}) = \begin{cases} 0 & \theta_L > \frac{\pi}{2} \\ 1 & \theta_L \leq \frac{\pi}{2} \end{cases}$$

If the parameters of Eqn (10) are known, after integrating the right-hand side, we can obtain the function with relative emissivity as the dependent variable, and observation direction  $(\theta_v, \phi_v)$  as the main independent variable, by dividing the radiation energy in the direction of (0,0) on both sides of the equation. In other words, we can get a so-called linear kernel driver model (William and Wan, 1998; Li and others, 2001), which is called the Relative Emissivity Distribution Function (REDF) and can be expressed as

$$\epsilon_r(\theta_v, \phi_v) = \sum_i f_i k_i(\theta_v, \phi_v) \tag{11}$$

Here  $f_i$  is a coefficient that can be functions with sea-ice surface parameters (e.g. gradient distribution and temperature distribution), and  $k_i(\theta_v, \phi_v)$  is a kernel function, whose main independent variable is  $(\theta_v, \phi_v)$ ; some other surface parameters are also included in some kernel driver models. In addition, if sea-ice surface reflection follows the principle of reciprocity, according to Kirchhoff's law, Eqn (11) can also be expressed as

$$\epsilon_r(\theta_v, \phi_v) = \frac{1 - \text{DHR}(\theta_v, \phi_v)}{1 - \text{DHR}(0, 0)} \tag{12}$$

where DHR is directional-hemispherical reflectance, which can use the hemisphere integral of linear kernel driver model BRDF in the incidence direction:

$$\text{DHR}(\theta_v, \phi_v) = \sum_i f_i^{\text{BRDF}} \widehat{k}_i^{\text{BRDF}}(\theta_v, \phi_v) \tag{13}$$

where  $f_i^{\text{BRDF}}$  is a coefficient,  $\widehat{k}_i^{\text{BRDF}}(\theta_v, \phi_v)$  is the hemisphere integral in the incidence direction and  $(\theta_v, \phi_v)$  is the dominated independent variable.

The linear kernel driver model BRDF can better describe the reflection of sea ice by considering the sea-ice surface roughness, but it neglects the non-isothermal surface temperature of sea ice, or assumes a higher precision at the isothermal surface. The relative emissivity in Eqn (11) is similar to e-emissivity, i.e. the ratio of the radiance of an ensemble of natural media to the radiance of that ensemble with the same temperature distribution, but with each element a black body (Norman and Becker, 1995). However, it is not identical to it. Equation (11) gives more consideration to the impact of surface morphology on radiation distribution characteristics and does not use the so-called radiation integral of each part of the black body as the denominator. Rather, it uses directional radiation energy as the denominator.  $k_i(\theta_v, \phi_v)$  includes the variable  $\epsilon_0$ ; the actual increment of emissivity due to temperature difference in pixels can be shown in  $\epsilon_0$  so that the emissivity in other directions can be obtained, although this is only an approximate calculation (Li and others, 2001).

*Linear kernel driver REDF model of smooth sea ice*

The surface of smooth sea ice observed herein is not an ideal plane, and has slight fluctuations (Table 1); in the freezing process, an absolute ideal plane is almost non-existent. Figure 9 shows the reflectance, emissivity and relative emissivity of an ideal plane at 8–13 μm TIR band. Reflectance

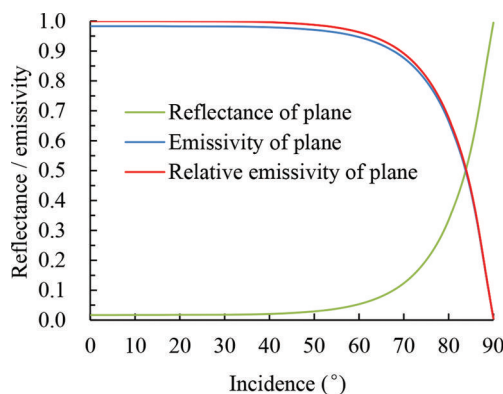


Fig. 9. Reflectance, emissivity and relative emissivity of a plane in TIR band.

is calculated using the Fresnel reflection equation

$$\gamma(\theta) = \frac{1}{2} \left[ \frac{\cos \theta - n \cos \theta'}{\cos \theta + n \cos \theta'} \right]^2 + \frac{1}{2} \left[ \frac{n \cos \theta - \cos \theta'}{n \cos \theta + \cos \theta'} \right]^2 \tag{14}$$

where  $\theta$  is the angle of incidence and  $n$  is the reflectance from air to ice. The average refractive index of ice at TIR band is 1.3.  $\theta'$  is the angle of refraction:

$$\theta' = \arcsin \left[ \frac{1}{n} \sin \theta \right]$$

Emissivity is calculated based on directional Kirchhoff's law:

$$\epsilon(\theta_v) = 1 - \rho_\Omega(\theta_v) \tag{15}$$

where  $\rho_\Omega(\theta_v)$  is directional-hemispherical reflectance. Relative emissivity is calculated using Eqn (6). Figure 9 shows that from 0° to Brewster's angle (when the unpolarized light is incident at Brewster's angle, the reflected light from the surface is perfectly polarized), the reflectance decreases slightly as the angle increases; when the viewing zenith angle is larger than Brewster's angle (~52.5°), reflectance increases rapidly with the increase in viewing zenith angle. The change in emissivity is contrary to this and increases slightly from 0° to Brewster's angle; when the viewing zenith angle is larger than Brewster's angle, emissivity decreases rapidly. The changing trend of relative emissivity is basically the same as that of emissivity.

According to the measured data in Figure 9, we use the linear kernel driver model to describe change in relative emissivity with change in viewing zenith angle. Currently, there are many kernel functions (Li and Zhou, 2002) describing the bidirectional reflectance distribution function (BRDF). The reflection of smooth sea ice is generally closely related only to incident zenith angle and viewing zenith angle. Combining the trend of observed data, we select the kernel function with incident zenith angle and viewing zenith angle as independent variables. Meanwhile, we give up the rough surface scattering model, which is physically meaningful but complicated, and obtain the relatively simple empirical linear kernel driver model REDF. The selected kernel function is

$$f_i^{\text{BRDF}}(\theta_s, \theta_v) = (1 - \cos \theta_v)^2 (1 - \cos \theta_s)^2 \tag{16}$$

where  $\theta_s$  is the incident zenith angle and  $\theta_v$  is the viewing zenith angle. The directional-hemispherical reflectance can be obtained by integrating  $\theta_s$ , and the integral is

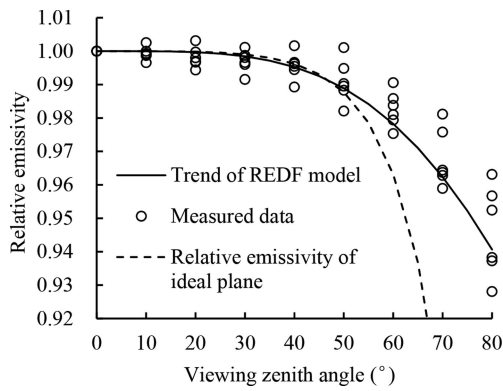


Fig. 10. Relative emissivity of smooth ice and REDF model.

expressed as

$$f^{BRDF}(\theta_v) = \frac{2}{9}(1 - \cos \theta_v)^2 \tag{17}$$

According to Eqns (15) and (17), when surface temperatures of smooth sea ice are uniform or slightly different, the emissivity of the viewing zenith angle in the direction of  $\theta_v$  can be expressed as

$$\varepsilon(\theta_v) = \varepsilon_0 \left[ 1 - \frac{2}{9}(1 - \cos \theta_v)^2 \right] \tag{18}$$

The second term in Eqn (18) reflects the strength of reflection; the actual smooth sea ice is also slightly rough. The use of Eqn (18) cannot accurately describe the multi-angular radiation characteristics of smooth sea ice. Therefore, we replace the coefficient 2/9 of the second item with a variable coefficient  $f$ , which can be expressed as a function with the slight roughness of smooth sea ice. Thus, Eqn (18) can be rewritten as

$$\varepsilon(\theta_v) = \varepsilon_0 \left[ 1 - f(1 - \cos \theta_v)^2 \right] \tag{19}$$

Both sides are divided by  $\varepsilon_0$  to obtain the expression for relative emissivity

$$\varepsilon_r(\theta_v) = 1 - f(1 - \cos \theta_v)^2 \tag{20}$$

The solid line in Figure 10 is the fitting curve based on measured data (circles) using a robust regression method; the value of  $f$  is 0.7675, the determination coefficient is 0.90 and RMSE is 0.006. It is shown that the fitting curve can better describe the change trend of relative emissivity of smooth sea ice with the viewing zenith angle, and an expression like Eqn (13) is suitable for describing the multi-angular radiation

Table 4. Candidate kernel functions describing relative emissivity of rough sea ice

No.	Kernel function
1	1
2	$\cos \theta_v$
3	$\sin \theta_v$
4	$\cos^2 \theta_v$
5	$\sin^2 \theta_v$
6	$\cos(\theta_v - \delta)$
7	$\sin(\theta_v - \delta)$
8	$\cos^2(\theta_v - \delta)$
9	$\sin^2(\theta_v - \delta)$

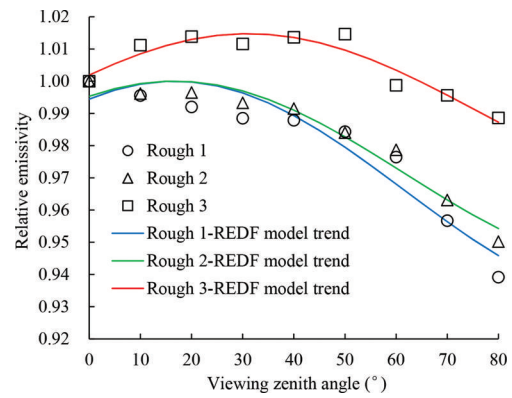


Fig. 11. Relative emissivity of rough ice and REDF model.

characteristics of smooth Bohai Sea ice. Thus, the emissivity in the known direction can be used to estimate the emissivity of other zenith angles, which helps further study the directional characteristics of rough sea-ice radiation.

Linear kernel driver REDF model of rough sea ice

The REDF of rough sea ice is not only related to the sea-ice surface roughness, but also to the the surface temperature distribution. If sea-ice surface temperatures at all locations are equal or slightly different, then the coefficient  $f$  in Eqn (20) can be adjusted to describe the REDF of rough sea ice. At the remote-sensing pixel scale, the distribution of actual temperature of the sea-ice surface cannot meet the above conditions. Equation (20) can also be substituted into Eqn (10) for complex integration to obtain the REDF of rough sea ice; however, there are some difficulties in accurate measurement of surface temperature distribution (especially the accurate measurement of surface skin ‘temperature’). Therefore, we give up use of Eqns (10) and (20) to describe the REDF of rough sea ice, and reselect a kernel function from the candidate kernel functions in Table 4.

Without considering the azimuth, three kernel functions in Table 4 are selected each time based on the measured data (the isotropic kernel is 1.0 and its coefficient is fixed at 1.0; kernel 2 describes relative emissivity characteristics of a plane; kernel 3 describes change in relative emissivity at different angles due to non-uniformity of roughness and temperature), the robust regression method is used to obtain the coefficient of each kernel, 28 fittings are conducted and the optimal combination is selected based on the error and coefficient of determination. In the final optimal combination the isotropic kernel is 1.0, kernel  $\sin^2(\theta - \delta)$  describing the relative emissivity characteristics of plane and kernel  $\cos^2(\theta - \delta)$  describing change in relative emissivity at different angles due to non-uniformity of roughness and temperature. The linear kernel driver model REDF of empirical relative emissivity of rough sea ice can then be expressed as

$$\varepsilon_r(\theta_v) = 1 + f_1 \sin^2(\theta_v - \delta) + f_2 \cos^2(\theta_v - \delta) \tag{21}$$

where  $f_1$  and  $f_2$  are coefficients.

The roughness and temperature distribution is associated with the viewing azimuth, which makes the measured radiation different for Rough 2 and Rough 3 (Fig. 11), but for a certain viewing zenith angle the average radiation of azimuth may be more stable and representative. In this paper, we ignore the influence of viewing azimuth, i.e. the REDF model assumes that the characteristic of sea-ice

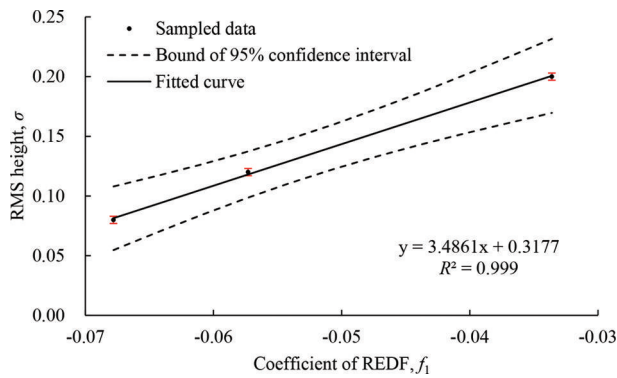


Fig. 12. Scatter diagram as a function of  $\sigma$  and  $f_1$ .

roughness was isotropic. The scattering points in Figure 11 (blocks, triangles and circles) are the averages of Figure 11 in the horizontal direction; the blue, green and red curves are fitting curves obtained using the robust regression method according to the measured data. Table 5 shows the parameter estimates of fitting curve. RMSEs are  $<0.01$ , and the determination coefficients ( $R^2$ ) are  $>0.900$ . It is worth noting that, with the increase in rms height, the absolute value of  $f_1$  decreases,  $f_2$  increases rapidly and  $\delta$  also increases. As roughness increases, the contribution of the second item [ $\cos^2(\theta_v - \delta)$ ] increases and the contribution of the first item [ $\sin^2(\theta_v - \delta)$ ] decreases in Eqn (21). When the gradient distribution is a unimodal distribution, the parameter  $\delta$  is somewhat related to the average gradient of a homeothermic patch of sea ice. Figure 12 and Table 5 show that Eqn (21) can better describe the REDF of Bohai Sea rough sea ice. Consideration should be given to building the relationship between  $\sigma$  and one or more parameters in Eqn (21) so that it can be used for estimation of sea-ice roughness. Figure 12 is a scatter diagram of  $\sigma$  and  $f_1$ , which shows that there exists a significant linear relationship between  $\sigma$  and  $f_1$  and the coefficient of determination of the fitted curve is 0.99. The RMSE of the fitted curve is 0.003 m. This shows that parameter  $f_1$  in the REDF model can be used to estimate the roughness ( $\sigma$ ) of sea ice.

However, the REDF is still a semi-empirical model, and was established under the assumption that the temperatures of all parts of the pixel are the same. In reality, a temperature difference exists between various parts of the pixel and may cause some errors. When the difference of the relative emissivities caused by the surface roughness is less than the difference caused by the surface temperature, the REDF model may not be suitable.

**DISCUSSION**

At present, the most commonly used thickness estimation model for Bohai Sea ice is the index estimation model based on the relationship between reflectance at visible light/near-infrared band and sea-ice thickness. The calculation method is (Su and Wang, 2012; Yuan and others, 2012)

$$\alpha(h) = \alpha_{\max} [1 - \kappa \exp(-\mu h)]$$

where  $h$  is sea-ice thickness,  $\alpha$  is reflectance at the visible light/near-infrared band, which changes with sea-ice thickness,  $\alpha_{\max}$  is the reflectance corresponding to sea ice with infinite thickness,  $\mu$  is the attenuation coefficient of reflectance and  $\kappa$  is a parameter associated with  $\alpha_{\max}$  and  $\alpha_{\text{sea}}$

Table 5. Estimates of parameters in a REDF model of rough sea ice

	$f_1$	$f_2$	$\delta$	RMSE	$R^2$	$\sigma$ m
Rough 1	-0.0678	$1.56 \times 10^{-9}$	0.2899	0.007	0.90	0.08
Rough 2	-0.0573	$3.08 \times 10^{-5}$	0.2904	0.004	0.95	0.12
Rough 3	-0.0336	0.0148	0.5417	0.003	0.91	0.20

(Yuan and others, 2012). If the reflectance  $\alpha$  is completely derived from volume scattering of sea ice, then the accuracy of sea-ice thickness estimation by this model will be improved. However, the reflectance  $\alpha$  inverted from remote-sensing data is mainly contributed to by two aspects: volume scattering of sea ice, and reflection of the sea-ice surface. It can be approximately expressed as

$$\alpha \approx w_s \alpha_s + w_v \alpha_v$$

where  $w_s$  and  $w_v$  are parameters connected with the physical properties of sea ice,  $\alpha_s$  is reflectance of the sea-ice surface and  $\alpha_v$  is reflectance of volume scattering of sea ice. Therefore, correction of reflectance  $\alpha$  can improve the inversion accuracy of thickness of rough sea ice. This paper suggests some possible and practical approaches to estimate sea-ice surface roughness, which is the most important parameter for estimating sea-ice surface reflectance. Sea-ice surface reflectance can be estimated from an analytical model (e.g. Kirchhoff approximation) or an empirical model. Correction of reflectance  $\kappa$  is also an important future task.

Of course, the approaches and models proposed herein also need to be tested and improved by application to specific remote-sensing data so that multi-angular TIR remote-sensing imagery can estimate Bohai Sea ice parameters in a more accurate and quantitative manner. In future work, the methods and models proposed in this study should be applied to specific remote-sensing data for testing and refinement to make the methodology more operational. For example, a sensor on board an aircraft or satellite can only make observations in two directions (fore and aft of the vehicle), whereas our REDF model was calculated based on measured radiation at four azimuths, which would not be easy to achieve at present. Currently our in situ measurements (e.g. ice surface roughness, brightness temperature) are carried out on a local scale. There may be a scale effect in the REDF model. In future research work, we will conduct more observations and surveys, and carry out actual estimate experiments on parameters of Bohai Sea ice based on multi-angular TIR remote-sensing images from aircraft and satellites. We will continue to improve the estimation accuracy of Bohai Sea ice thickness in conjunction with multi-angular optical remote-sensing experiments, and to carry out large-scale, real-time and highly accurate estimation of Bohai Sea ice thickness.

**CONCLUSIONS**

After analysis of the results of multi-angular TIR radiation field observations and tests of smooth and rough sea ice in Liaodong Bay, Bohai Sea, we conclude:

1. The relative emissivity of smooth sea ice decreases as the viewing zenith angle increases ( $-0.003$  to

- 0.001 degree<sup>-1</sup>, viewing zenith angle >50°); the shape of the relative emissivity curve is very similar to the shape of the relative emissivity curve for an ideal plane;
- The relative emissivity of rough sea ice is affected by roughness, surface temperature distribution and other parameters; the larger the roughness, the stronger and more complex is the anisotropy of relative emissivity (the average being at 0.036);
  - The theoretical derivation and fitting of measured data both show that the linear kernel driver model REDF can be used to describe the emission characteristics of sea ice. Thus, we obtain the coefficients in the linear kernel driver REDF models of smooth and rough sea ice based on the measured data. Although the relative emissivity is not the emissivity of sea ice in a physical sense, it is closely related to the roughness, surface temperature distribution and other parameters of sea ice. Multi-angular TIR remote sensing has a certain potential in the inversion surface roughness of sea ice, especially for sea ice with roughness from several centimetres to tens of centimetres.

## ACKNOWLEDGEMENTS

This research was supported by the the Projects of State Key Laboratory of Earth Surface Progress and Resource Ecology (No. 2010-KF-08), National High Technology Research and Development Program of China (No. 2011AA100505) and the National Key Technology R&D Program of China (No. 2012BAK02B03). We express our appreciation to the individuals in the working group for help during the research and to the reviewers for helpful comments and suggestions.

## REFERENCES

- Comiso JC (2001) Satellite-observed variability and trend in sea-ice extent, surface temperature, albedo and clouds in the Arctic. *Ann. Glaciol.*, **33**, 457–473 (doi: 10.3189/172756401781818617)
- Ding D (1999) *An introduction to engineering sea ice*. China Ocean Press, Beijing [in Chinese]
- Drüe C and Heinemann G (2005) Accuracy assessment of sea-ice concentrations from MODIS using in-situ measurements. *Remote Sens. Environ.*, **95**(2), 139–149
- García V, Mira M, Valor E, Caselles V, Coll C and Galve JM (2009) Angular dependence of the emissivity of bare soils in the thermal infrared. In *IGARSS 2009, International Geoscience and Remote Sensing Symposium, 12–17 July 2009, Cape Town, South Africa*. Institute of Electrical and Electronics Engineers, Piscataway, NJ, 133–136
- Groves JE and Stringer WJ (1991) The use of AVHRR thermal infrared imagery to determine sea ice thickness within the Chukchi Polynya. *Arctic*, **44**(Suppl. 1), 130–139
- Gu W and 6 others (2013) Spatial distribution characteristics of sea-ice-hazard risk in Bohai, China. *Ann. Glaciol.*, **54**(62), 73–79 (doi: 10.3189/2013AoG62A303)
- Kaleschke L, Tian-Kunze X, Maaß N, Mäkynen N and Drusch M (2012) Sea ice thickness retrieval from SMOS brightness temperatures during the Arctic freeze-up period. *Geophys. Res. Lett.*, **39**(5) (doi: 10.1029/2012GL050916)
- Kuenzer C and Dech S (2013) *Thermal infrared remote sensing*. Springer, Berlin, 299–304
- Launiainen J and Cheng B (1998) Modelling of ice thermodynamics in natural water bodies. *Cold Reg. Sci. Technol.*, **27**, 153–178
- Li L, Liu C, Gu W, Xu Y and Tao J (2012) Research progress and problems in desalination and utilization of sea ice in Bohai Sea. *Mar. Sci. Bull.*, **31**(1), 105–112 [in Chinese]
- Li S and Zhou X (2002) Deriving reciprocal kernel functional expression of Antarctic sea ice surface BRDF from field measurements. In *IGARSS 2002, International Geoscience and Remote Sensing Symposium, 24–28 June 2002, Toronto, Canada*. Institute of Electrical and Electronics Engineers, Piscataway, NJ, 2173–2175
- Li X, Strahler AH and Friedl MA (1999) A conceptual model for effective directional emissivity from nonisothermal surfaces. *IEEE Trans. Geosci. Remote Sens.*, **37**(5), 2508–2517
- Li X, Wang J, Wang J and Liu Q (2001) *Multi angle and thermal infrared remote sensing of the earth*. Science Press, Beijing, 71–150 [in Chinese]
- Li ZL and 7 others (2013) Satellite-derived land surface temperature: current status and perspectives. *Remote Sens. Environ.*, **131**, 14–37
- Liu C, Gu W, Chao J, Li L, Yuan S and Xu Y (2013) Spatio-temporal characteristics of the sea-ice volume of the Bohai Sea, China, in winter 2009/10. *Ann. Glaciol.*, **54**(62), 97–104 (doi: 10.3189/2013AoG62A305)
- Luo Y, Wu H, Zhang Y, Sun C and Liu Y (2004) Application of the HY-1 satellite to sea ice monitoring and forecasting. *Acta Oceanol. Sin.*, **23**(2), 7–18 [in Chinese]
- Masahiro H and 10 others (2006) In-situ measured spectral directional emissivity of snow and ice in the 8–14 μm atmospheric window. *Remote Sens. Environ.*, **100**, 486–502
- Norman J and Becker F (1995) Terminology in thermal infrared remote sensing of natural surface. *Agric. Forest Meteorol.*, **77**, 153–176
- Omstedt A (1990) A coupled one-dimensional sea ice-ocean model applied to a semi-enclosed basin. *Tellus*, **42A**, 568–582
- Su H and Wang Y (2012) Using MODIS data to estimate sea ice thickness in the Bohai Sea (China) in the 2009–2010 winter. *J. Geophys. Res. Oceans*, **117**(C10)
- William CS and Wan Z (1998) BRDF models to predict spectral reflectance and emissivity in the thermal infrared. *IEEE Trans. Geosci. Remote Sens.*, **36**(1), 214–225
- Wu L, Wu H, Sun LT, Zhang YF, Liu Y and Wei XQ (2006) Retrieval of sea ice in the Bohai Sea from MODIS data. *Period. Ocean Univ. China*, **36**(2), 173–179
- Xu X (2006) *Physical theory of remote sensing*. Peking University Press, Beijing [in Chinese]
- Yang G (2000) *Sea ice engineering*. Petroleum Industry Press, Beijing [in Chinese]
- Yuan S and 6 others (2012) The estimate of sea ice resources quantity in the Bohai Sea based on NOAA/AVHRR data. *Acta Oceanol. Sin.*, **31**(1), 33–40 (doi: 10.1007/s13131-012-0173-4)
- Zheng X, Qiu K and Lu F (1998) Quantitative calculation of sea ice over the Bohai Sea using NOAA/AVHRR imagery. *J. Appl. Meteorol. Sci.*, **9**(3), 359–363 [in Chinese]

MS received 31 August 2014 and accepted in revised form 26 June 2015